Effects of multichance fission on isotope dependence of fission fragment mass distributions at high energies

S. Tanaka,[1,2] Y. Aritomo,[1] Y. Miyamoto,[1] K. Hirose,[2] and K. Nishio[2]
[1]*Graduate School of Science and Engineering, Kindai University, Higashi-Osaka 577-8502, Japan*
[2]*Advanced Science Research Center, Japan Atomic Energy Agency, Tokai, Ibaraki 319-1195, Japan*

(Received 17 October 2019; published 13 December 2019)

Fission fragment mass distributions of $^{234–240}$U, $^{236–242}$Np, and $^{238–244}$Pu are studied using the Langevin approach in the wide excitation energy range as $E^* = 15$–55 MeV. In the present calculation, neutron emission before fission, so-called multichance fission, was introduced. The calculated results well demonstrated the experimental data, which shows the double-peak structure up to the highest excitation energies and the clear dependence on the initial fissioning nuclides. The trend is nicely correlated with the neutron binding energy of the compound nucleus that dominates the neutron emission probability before fission.

DOI: 10.1103/PhysRevC.100.064605

I. INTRODUCTION

Since the discovery of nuclear fission of uranium in 1938 [1,2], the phenomenon has been widely used to generate energy in atomic power plants. Using the dedicated nuclear reactors, neutrons from the reactor core are also widely used for many applications, such as neutron capture therapy and material science. Understanding of the fission process itself is important in other fields of science. For example, the existence of nuclei in the superheavy element region is regulated by the stability of the nucleus against fission. The role of so-called fission recycle in the astrophysical nucleosynthesis is nowadays extensively discussed [3,4], which might impact the abundance of the chemical elements and also the heaviest elements produced in neutron-star merger.

Concerning the atomic energy applications, one of the most important issues is to reduce the already existing and newly produced nuclear waste, particularly the long-lived minor actinides (MAs). The use of accelerator-driven systems (ADS), for example [5], is considered as one of the viable options for the incineration and/or transmutation of the long-lived minor actinides into short-lived fission products. In the ADS approach, energetic spallation neutrons, produced via high-energy proton impact on a heavy target material such as lead and/or bismuth, could be used to irradiate the fissionable MAs. This leads to fission with higher and more broadly distributed excitation energies in comparison to those in the thermal-neutron-induced fission in a traditional power reactor. Thus, understanding of fission at high excitation energy is important for nuclear-data evaluations related to ADS developments.

The key phenomena, which does not occur in low-energy fission but happens in high-energy fissions, is the neutron evaporation before fission. The effects of the so-called multichance fission (MCF) on the fission fragment mass distributions (FFMDs) are schematically shown in Fig. 1. The compound nucleus ^{238}U with an initial excitation energy $E^* = 35$ MeV in this example can decay either via first-chance fission, or via single neutron emission, leading to the less excited ^{237}U. The latter nucleus can decay again either by fission (thus, second-chance fission) or by neutron evaporation; the competition between fission and neutron emission continues until the excitation energy of the corresponding daughter nucleus (or residual nucleus) drops below the fission barrier. The shape of the FFMD at each fission chance is also shown schematically in this figure, with predominantly symmetric fission for the initial compound nucleus ^{238}U, and dominant asymmetric fission for subsequent higher-order fission chances, due to the revival of the shells responsible for mass asymmetry in fission. In the current experimental setup, number of neutron emission before fission cannot be unambiguously determined event by event, thus the experimentally observed FFMDs are usually observed as a mixture of different fission chances.

Recently, effects of MCF has been discussed using a statistical model to determine the neutron-fission competition and the Langevin calculation to describe fission [6]. It was concluded that the apparent-asymmetric fission in U, Np, and Pu nuclei observed in experiment [6–8] at high excitation energies originates from higher fission chances after evaporation of several neutrons. In this paper, we extend the similar calculation to other nuclei with an updated model with a higher prediction accuracy. As a result, the experimentally observed trend of FFMDs, characterized by the peak-to-valley ratio of its double-humped shape and mass asymmetry, in terms of neutron and proton number of the initial compound nucleus, are nicely reproduced. Accordingly, the results unveiled the FFMD of for each excitation energy, which cannot be determined solely by the experiments.

II. MODEL

We use the fluctuation-dissipation model and employ Langevin equations to calculate the evolution of nuclear shape with time [9,10]. The nuclear shape is defined by the two-center shell model parametrization [11,12], which has three

deformation parameters, z, δ, and α to serve as collective coordinates, abbreviated as $q = \{z, \delta, \alpha\}$. The symbol z is the distance between two potential centers, the δ denotes the deformation of the fragments, and $\alpha = (A_1 - A_2)/(A_1 + A_2)$ is the mass asymmetry of the two fragments [9], where A_1 and A_2 are the mass numbers of heavy and light fragments.

For a given value of the temperature of a system T, the potential energy is defined as a sum of the liquid-drop (LD) part and a microscopic (SH) part:

$$\begin{aligned} V(q,T) &= V_{\rm LD}(q) + V_{\rm SH}(q,T), \\ V_{\rm LD}(q) &= E_{\rm S}(q) + E_{\rm C}(q), \\ V_{\rm SH}(q,T) &= [\Delta E_{\rm shell}(q) + \Delta E_{\rm pair}(q)]\Phi(T), \\ \Phi(T) &= \exp\left(-\frac{aT^2}{E_d}\right). \end{aligned} \tag{1}$$

Here, the potential energy $V_{\rm LD}$ is calculated with the finite-range liquid drop model [13], given as a sum of the surface energy $E_{\rm S}$ and the Coulomb energy $E_{\rm C}$. The microscopic energy $V_{\rm SH}$ at $T = 0$ is calculated as the sum of the shell correction energy $\Delta E_{\rm shell}$, evaluated by the Strutinski method [14,15], and the pairing correlation correction energy $\Delta E_{\rm pair}$ [15,16]. The shell correction energy has a temperature dependence expressed by a factor $\Phi(T)$ in which the shell damping energy E_d is chosen as 20 MeV [17] and a is the level density parameter [10,18]. To define the potential of the two-center shell model [11,12], a neck parameter of $\epsilon = 0.35$ ($0 \leqslant \epsilon \leqslant 1$) [19] has been routinely used [6,7,10,20–22]. However, this value is not appropriate for heavier actinide nuclides as pointed out in Refs. [6,23]. We adopt the optimal ϵ values following the empirical relation

$$\epsilon(A_c) = 0.01007A_c - 1.94, \tag{2}$$

where A_c is the mass of the fissioning nucleus [23].

The multidimensional Langevin equations [9] are given as

$$\begin{aligned} \frac{dq_i}{dt} &= (m^{-1})_{ij}p_j, \\ \frac{dp_i}{dt} &= -\frac{\partial V}{\partial q_i} - \frac{1}{2}\frac{\partial}{\partial q_i}(m^{-1})_{jk}p_jp_k \\ &\quad - \gamma_{ij}(m^{-1})_{jk}p_k + g_{ij}R_j(t), \end{aligned} \tag{3}$$

where $q_i = \{z, \delta, \alpha\}$ and $p_i = m_{ij}dq_i/dt$ is a momentum conjugate to coordinate q_i. In the Langevin equation, m_{ij} and γ_{ij} are the shape-dependent collective inertia and the friction tensors, respectively. The wall-and-window one-body dissipation [24–26] is adopted for the friction tensor. The normalized random force $R_i(t)$ is assumed to be that of white noise, i.e.,

$$\langle R_i(t)\rangle = 0, \quad \langle R_i(t_1)R_j(t_2)\rangle = 2\delta_{ij}\delta(t_1 - t_2). \tag{4}$$

The strength of the random force g_{ij} is related to the friction tensor γ_{ij} by the classical Einstein relation,

$$\sum_k g_{ij}g_{jk} = \gamma_{ij}T. \tag{5}$$

The random properties introduced in Eqs. (3)–(5) gives different trajectories on the potential energy space event by event, creating the fission fragment mass distribution by accumulating enough number of different trajectories, which can be directly compared to the experimental data. In each trajectory, fission is defined as the case that nucleus reaches the scission point on the potential energy surface.

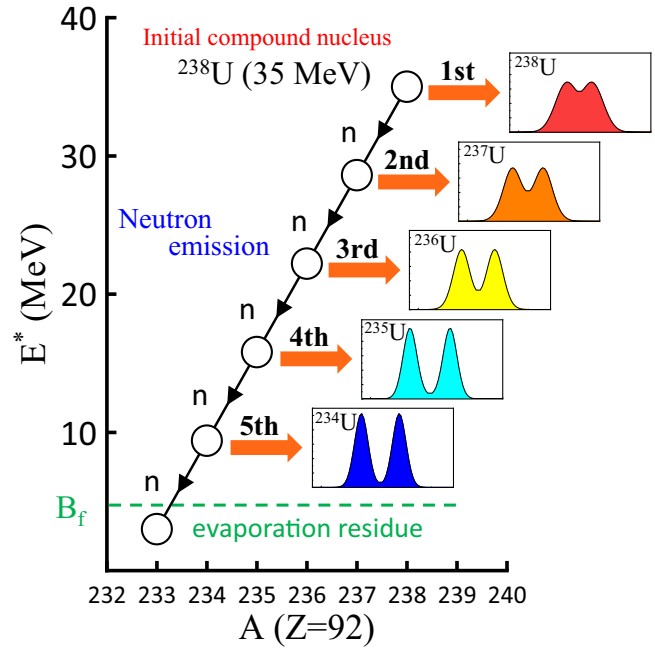

FIG. 1. A conceptual view of multichance fission for the case of ^{238}U, see details in the text.

III. RESULT AND DISCUSSION

Figure 2 shows the potential energy surface for ^{236}U, plotted on the z-α plane. Figures 2(a) and 2(b) correspond to the low ($E^* = 15$ MeV) and high excitation energies ($E^* = 45$ MeV), respectively, where the shell correction energy and its smearing with the excitation energy [Eq. (1)] can be comprehended. For the low excitation [Fig. 2(a)], the system has two saddle points; the inner (first) saddle point located at the mass symmetry $\alpha = 0.0$ and the outer (second) saddle point standing at the mass asymmetry $\alpha = 0.2$. As shown in the sample trajectory, calculated by the Langevin equations [Eq. (3)] and indicated in this figure, the nuclear shape evolves with time by overcoming these saddle points. For the low-energy fission, the mass asymmetry is almost fixed at the second saddle point, without changing it during the descent from the saddle to scission, giving a clear double-humped fission-fragment mass distribution [see Fig. 2(a)]. For the high-energy fission, almost the single-Gaussian-like shape of the FFMD is given [Fig. 2(b)].

Importance of the neutron-emission before fission (multichance fission: MCF) on the FFMD are explained in Fig. 3, by showing the results for ^{238}U at the initial excitation energy of 35 MeV. Figure 3(a) is the calculation without introducing the concept of MCF, no neutron evaporation from the compound nucleus. In contrast to the clear double-humped structure of the experimental data, the calculation shows significantly smaller peak-to-valley (P/V) ratio in the FFMD.

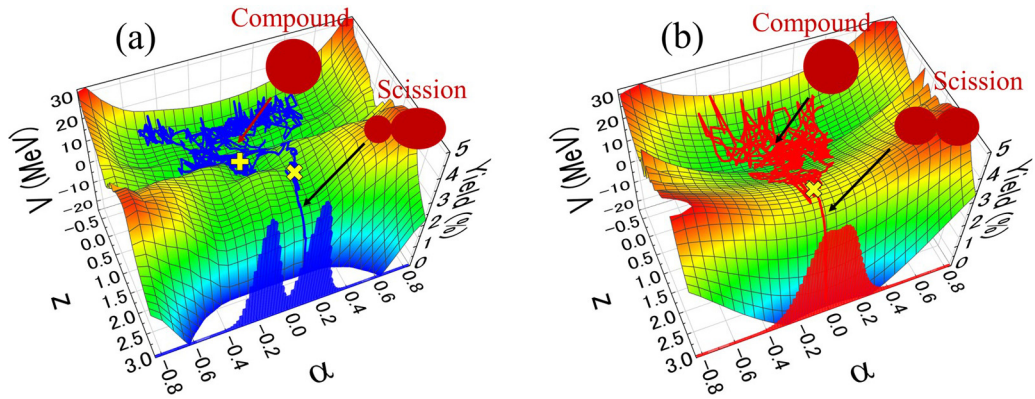

FIG. 2. Sample trajectory projected on potential energy surface, which is the z-α plane at $\delta = 0.2$ and an example of calculation results of FFMDs for ^{236}U at (a) $E^* = 15$ MeV and at (b) $E^* = 45$ MeV. In (a) the first and second saddle points are marked by the symbols "+" and "×", respectively.

Also the mass-asymmetry of the peak position, $A_L/A_H \approx 108u/130u$, is apparently smaller than the measurement ($A_L/A_H \approx 98u/140u$). On the other hand, the experimental data are nicely reproduced by including the MCF concept as shown in Fig. 3(b) in terms P/V ratio and location of the peaks. The calculated FFMDs for individual fission chances are also shown by the dashed curves with different colors, where the fraction (probability) of each fission chance is determined using a statistical model code GEF [27]. The reduction of the excitation energy of the compound nucleus for each neutron emission was calculated using neutron binding energies [28] and an average neutron kinetic energy, $\approx$ 1.9 MeV, obtained by the PACE2 code [29]. The finally obtained FFMD, which can be compared to the experimental data is given by summing up all the possible fission chance curves. It is evident that the mass-asymmetric shape is largely created by the third-, fourth-, and fifth-chance fissions (^{236,235,234}U), having dominant yield in total, than the first- and second-chance fissions (^{238,237}U).

The same calculation procedure was performed for the 21 compound nuclides ($^{234–240}$U, $^{236–242}$Np, and $^{238–244}$Pu) as well as their dependence on the average-excitation energy, ranging from $E^* = 15$–55 MeV, as shown in Fig. 4. Here, the results are compared to the experimental data taken using the multinucleon transfer (MNT) reactions of ^{18}O + ^{238}U [6] for $^{237–240}$U, $^{239–242}$Np, $^{242–244}$Pu, and ^{18}O + ^{237}Np [8] for $^{234–236}$U, $^{236–238}$Np, $^{238–241}$Pu, carried out at the JAEA Tokai tandem facility. For nuclides available from both reactions, we cite the one with the smaller statistical error. Note that experimental data for ^{244}Pu at $E^* = 15$ MeV are not available due to the limited number of accumulated events. In contrast to the calculation without MCF (blue curves), the results with MCF (red curves) well reproduce the experimental data for all the studied nuclides as well as their excitation-energy dependence within the experimental uncertainties, especially the double-humped shape of the FFMD remaining up to the highest energies are noteworthy. Furthermore, growing P/V ratio toward heavier-mass isotopes in each element (U, Np, Pu), most clearly showing up at $E^* \geqslant 35$ MeV, are well described. In addition, for a certain number of neutrons N contained in the initial compound nucleus, the heavier element shows the smaller P/V ratio when one compare the spectra at a certain excitation energy (see the fissioning nuclei with $N = 144$–148). These systematic trends, found clearly by the MNT fission measurements, are strongly correlated with the neutron-emission probability from the compound nucleus, rather than the difference of the fission process between the studied nuclides, as

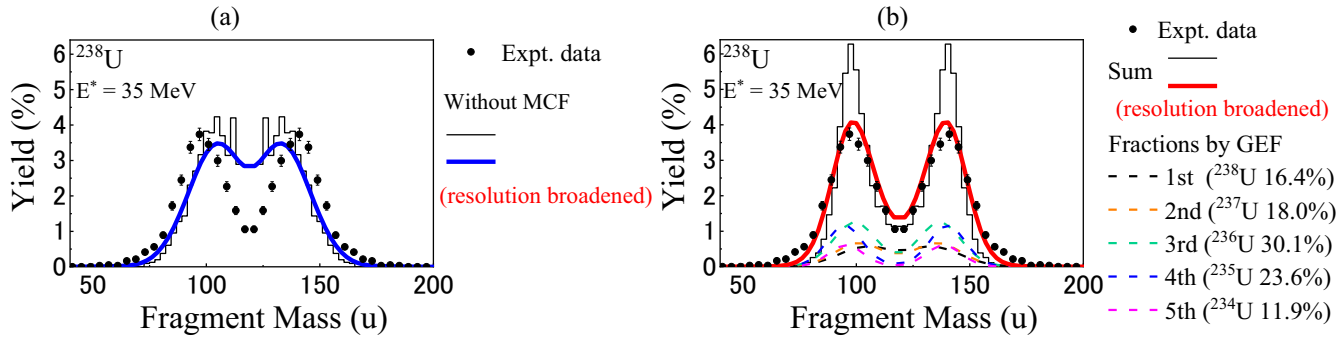

FIG. 3. Calculated results for fission fragment mass distribution of ^{238}U* at the initial excitation energy $E^* = 35$ MeV without and with taking into account the MCF, black thin curve shown in (a) and (b), respectively. The results are compared with the experimental data [6] (solid circles). In (b), the calculated FFMDs for all the fission chances (dashed curves with different colors) are shown. For comparison with the experimental data, the calculated results are broadened with the experimental mass resolution, as shown by the blue/red thick curve.

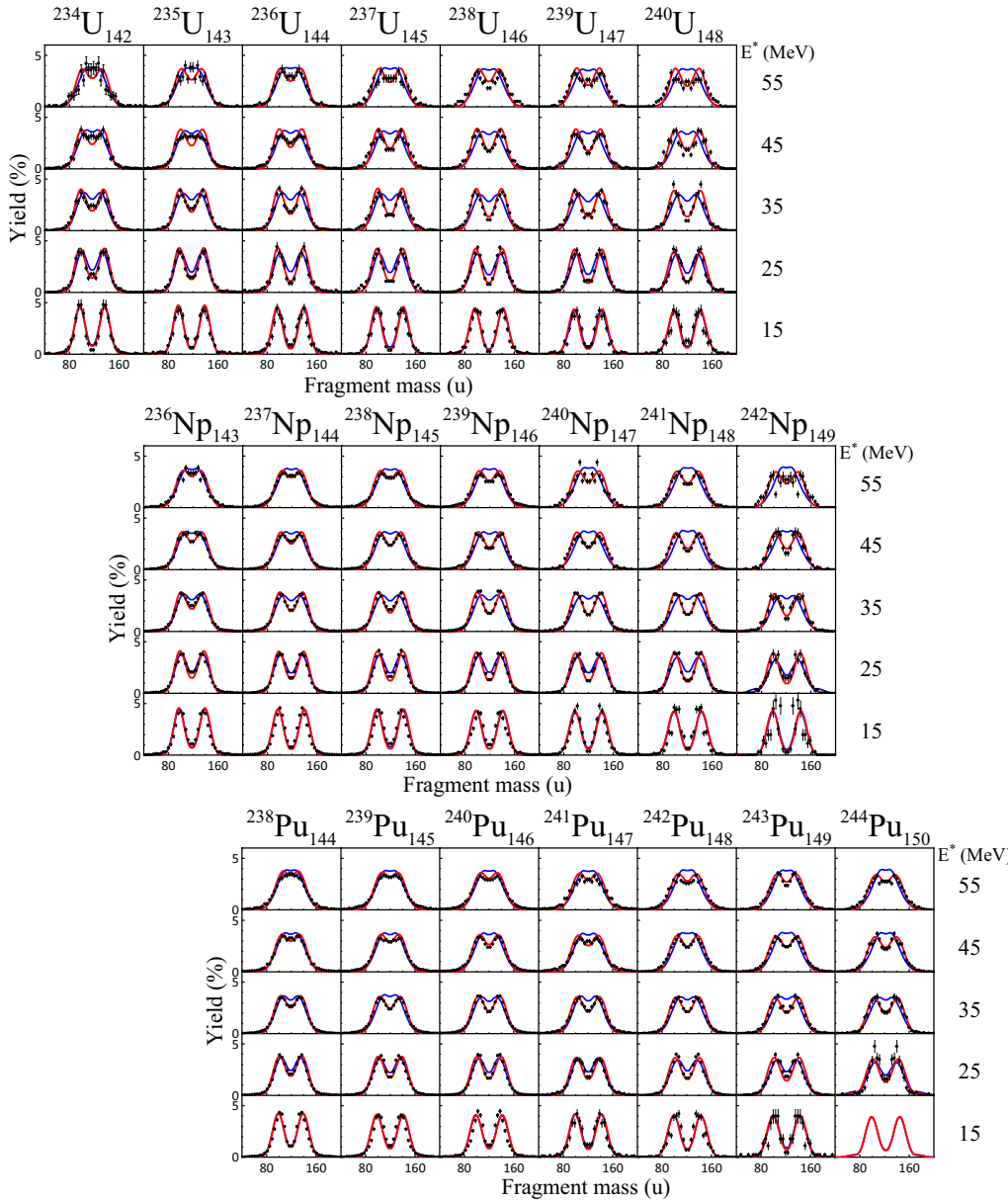

FIG. 4. Comparison of the measured FFMDs for uranium, neptunium and plutonium isotopes (solid circles) [6,8] with the Langevin calculations from the different assumption. The red and blue curves are the calculation with and without taking into the MCF concept, respectively. The average excitation-energy for each 10-MeV excitation-energy bin is shown on the right-hand side. Panels for uranium, neptunium and plutonium are arranged so that the fissioning nuclides with the same neutron number (N) are aligned in the same column.

evidenced by the FFMDs with blue curves that show almost the similar shapes over the nuclides at a certain excitation energy.

Table I shows neutron binding energy [28] and the mean number of neutron emission before fission calculated by the GEF code [27] for 21 nuclides studied in this work. As shown in Table I, for a certain element isotopes, it is evident that prescission neutron multiplicity $\langle \nu_{\rm pre} \rangle$ increases with the compound-nucleus mass due to decrease of the neutron binding energy. This effect is also reported in Ref. [30] that multiple neutron emission increase with the mass number A for $^{233–239}$U (see Fig. 14 in Ref. [30]). The competition between neutron emission and fission also depends largely on the fission barrier height. For the studied nuclei in this paper, however, the fission barrier heights do not change very much with each other as follows. The semiempirical GEF model estimate the fission barrier height as the sum of the macroscopic fission barrier and the shell-correction energy in the ground state, making use of the topographic theorem [31,32]. This model well reproduces isotopic dependence of the measured fission barriers, both for the inner and the outer barriers, $E_{\rm A}$ and $E_{\rm B}$, as shown in Ref. [27], Fig. 7 and Fig. 8. For the nuclides studied in the present analysis, the inner and the outer barriers are nearly the same for uranium isotopes ($^{234–240}$U) with values $E_{\rm A} = 5.44–6.04$ MeV. The neptunium and plutonium isotopes ($^{236–242}$Np, $^{238–244}$Pu) have $E_{\rm A}$ values

TABLE I. Two-neutron binding energy (S_{2n} in MeV) [28], fission barriers used in GEF (B_f in MeV) [27], and mean number of neutron emission before fission $\langle \nu_{pre} \rangle$ calculated by GEF are tabulated for each fissionig nucleus ${}^{A}Z_{N}$ and initial excitation energy E^*(MeV). For B_f, the only the higher barrier is listed (1: inner, 2: outer).

Z	$A(N)$	S_{2n}	B_f	E^*	$\langle \nu_{pre} \rangle$	Z	$A(N)$	S_{2n}	B_f	E^*	$\langle \nu_{pre} \rangle$	Z	$A(N)$	S_{2n}	B_f	E^*	$\langle \nu_{pre} \rangle$
92	234(142)	12.60	5.69[1]	15	0.16	93	236(143)	12.66	6.08[1]	15	0.16	94	238(144)	12.88	5.65[1]	15	0.09
				25	0.69					25	0.57					25	0.45
				35	1.22					35	1.04					35	0.90
				45	1.72					45	1.51					45	1.35
				55	2.20					55	1.96					55	1.81
	235(143)	12.14	5.95[1]	15	0.29		237(144)	12.30	5.70[1]	15	0.14		239(145)	12.65	6.08[1]	15	0.17
				25	0.87					25	0.65					25	0.61
				35	1.47					35	1.19					35	1.10
				45	2.00					45	1.69					45	1.60
				55	2.52					55	2.20					55	2.08
	236(144)	11.84	5.76[1]	15	0.26		238(145)	12.11	6.19[1]	15	0.29		240(146)	12.18	5.70[1]	15	0.12
				25	0.92					25	0.83					25	0.61
				35	1.61					35	1.42					35	1.19
				45	2.21					45	1.97					45	1.74
				55	2.75					55	2.48					55	2.26
	237(145)	11.67	6.06[2]	15	0.41		239(146)	11.70	5.68[1]	15	0.14		241(147)	11.77	5.97[1]	15	0.22
				25	1.14					25	0.78					25	0.75
				35	1.85					35	1.51					35	1.37
				45	2.49					45	2.10					45	1.96
				55	3.06					55	2.66					55	2.51
	238(146)	11.28	5.71[2]	15	0.26		240(147)	11.38	5.97[1]	15	0.25		242(148)	11.55	5.61[1]	15	0.14
				25	0.99					25	0.94					25	0.73
				35	1.97					35	1.62					35	1.43
				45	2.61					45	2.30					45	2.06
				55	3.25					55	2.90					55	2.65
	239(147)	10.96	5.94[2]	15	0.35		241(148)	11.19	5.63[1]	15	0.22		243(149)	11.34	5.89[1]	15	0.24
				25	1.29					25	0.88					25	0.92
				35	1.97					35	1.71					35	1.57
				45	2.80					45	2.37					45	2.24
				55	3.48					55	3.03					55	2.87
	240(148)	10.73	5.59[2]	15	0.25		242(149)	10.94	5.98[1]	15	0.35		244(150)	11.05	5.49[1]	15	0.14
				25	0.79					25	1.27					25	0.80
				35	1.95					35	1.80					35	1.61
				45	2.69					45	2.53					45	2.27
				55	3.53					55	3.23					55	2.94

larger than E_B, and the $E_A = 5.63$–6.19 MeV (Np) and $E_A = 5.49$–6.08 MeV (Pu) are close to those for ${}^{234-240}$U.

The calculation results without the MCF (blue curves in Fig. 4) show predominantly symmetric fission due to the washing out of the shell structure already at the excitation energy ≈45 MeV for all the studied nuclides. We also note that the shell damping energy $E_d = 20$ MeV, which has been routinely used to describe heavy-ion reaction and fission process, and thus used in this model, can account for the experimental data, without introducing unexpectedly large values.

IV. SUMMARY

To conclude, even though multichance fission (MCF) is a well-established concept to explain the stepwise structure of the fission probability (fission cross section) appearing periodically in the excitation function, so far its effects on fission-fragment mass distributions has not been fully investigated. This is mainly due to the absence of systematic data and proper fission model, which can generate FFMDs with enough accuracy. This difficulty was overcome/solved by exploiting the novel approach of multinucleon transfer (MNT) reactions in experiment and Langevin approach in calculation. In this study, calculation which takes into account the MCF explained the large set of experimental data from the MNT-induced fissions. Our results also suggest that the consideration of MCF is essential to interpret other fission observables.

ACKNOWLEDGMENTS

The Langevin calculations were performed using the cluster computer system (Kindai-VOSTOK), which is supported by Japan Society for the Promotion of Science (JSPS) KAKENHI Grant No. 17K05455.

[1] O. Hahn and F. Straßmann, Naturwissenschaften **27**, 11 (1939).
[2] L. Meitner and O. R. Frisch, Nature (London) **143**, 239 (1939).
[3] I. V. Panov, E. Kolbe, B. Pfeiffer, T. Rauscher, K.-L. Kratz, and F.-K. Thielemann, Nucl. Phys. A **747**, 633 (2005).
[4] I. Petermann, K. Langanke, G. Martínez-Pinedo, I. V. Panov, P. G. Reinhard, and F. K. Thielemann, Eur. Phys. J. A **48**, 122 (2012).
[5] T. Mukaiyama, T. Takizuka, M. Mizumoto, Y. Ikeda, T. Ogawa, A. Hasegawa, H. Takada, and H. Takano, Prog. Nucl. Energy **38**, 107 (2001).
[6] K. Hirose, K. Nishio, S. Tanaka, R. Leguillon, H. Makii, I. Nishinaka, R. Orlandi, K. Tsukada, J. Smallcombe, and M. J. Vermeulen *et al.*, Phys. Rev. Lett. **119**, 222501 (2017).
[7] R. Leguillon *et al.*, Phys. Lett. B **761**, 125 (2016).
[8] M. J. Vermeulen *et al.* (unpublished).
[9] Y. Aritomo and M. Ohta, Nucl. Phys. A **744**, 3 (2004).
[10] Y. Aritomo, S. Chiba, and F. Ivanyuk, Phys. Rev. C **90**, 054609 (2014).
[11] J. Maruhn and W. Greiner, Z. Phys. **251**, 431 (1972).
[12] K. Sato, A. Iwamoto, K. Harada, S. Yamaji, and S. Yoshida, Z. Phys. A **288**, 383 (1978).
[13] H. J. Krappe, J. R. Nix, and A. J. Sierk, Phys. Rev. C **20**, 992 (1979).
[14] V. M. Strutinsky, Nucl. Phys. A **95**, 420 (1967).
[15] V. M. Strutinsky, Nucl. Phys. A **122**, 1 (1968).
[16] S. G. Nilsson, C. F. Tsang, A. Sobiczewski *et al.*, Nucl. Phys. A **131**, 1 (1969).
[17] A. V. Ignatyuk, G. N. Smirenkin, and A. S. Tishin, Sov. J. Nucl. Phys. **21**, 255 (1975).
[18] J. Toke and W. J. Swiatecki, Nucl. Phys. A **372**, 141 (1981).
[19] S. Yamaji, H. Hofmann, and R. Samhammer, Nucl. Phys. A **475**, 487 (1988).
[20] Y. Aritomo and S. Chiba, Phys. Rev. C **88**, 044614 (2013).
[21] M. D. Usang, F. A. Ivanyuk, C. Ishizuka, and S. Chiba, Phys. Rev. C **94**, 044602 (2016).
[22] M. D. Usang, F. A. Ivanyuk, C. Ishizuka, and S. Chiba, Phys. Rev. C **96**, 064617 (2017).
[23] Y. Miyamoto, Y. Aritomo, S. Tanaka, K. Hirose, and K. Nishio, Phys. Rev. C **99**, 051601(R) (2019).
[24] J. Blocki, Y. Boneh, J. R. Nix, J. Randrup, M. Robel, A. J. Sierk, and W. J. Swiatecki, Ann. Phys. (NY) **113**, 330 (1978).
[25] J. R. Nix and A. J. Sierk, Nucl. Phys. A **428**, 161c (1984).
[26] H. Feldmeier, Rep. Prog. Phys. **50**, 915 (1987).
[27] K.-H. Schmidt, B. Jurado, C. Amouroux, and C. Schmitt, Nucl. Data Sheets **131**, 107 (2016).
[28] P. Möller, A. J. Sierk, T. Ichikawa, and H. Sagawa, At. Data Nucl. Data Tables **109–110**, 1 (2016).
[29] A. Gavron, Phys. Rev. C **21**, 230 (1980).
[30] M. Sin, R. Capote, M. W. Herman, and A. Trkov, Nucl. Data Sheets **139**, 138 (2017).
[31] W. D. Myers and W. J. Swiatecki, Nucl. Phys. A **601**, 141 (1996).
[32] A. V. Karpov, A. Kelic, and K.-H. Schmidt, J. Phys. G: Nucl. Part. Phys. **35**, 035104 (2008).